Lifshitz transition and Van Hove singularity in a three-dimensional topological Dirac semimetal

Su-Yang Xu,[1] Chang Liu,[1,2] I. Belopolski,[1] S. K. Kushwaha,[3] R. Sankar,[4] J. W. Krizan,[3] T.-R. Chang,[5] C. M. Polley,[6] J. Adell,[6] T. Balasubramanian,[6] K. Miyamoto,[7] N. Alidoust,[1] Guang Bian,[1] M. Neupane,[1] H.-T. Jeng,[5,8] C.-Y. Huang,[9] W.-F. Tsai,[9] T. Okuda,[7] A. Bansil,[10] F. C. Chou,[4] R. J. Cava,[3] H. Lin,[11] and M. Z. Hasan[1]

[1]*Laboratory for Topological Quantum Matter and Spectroscopy (B7), Department of Physics, Princeton University, Princeton, New Jersey 08544, USA*

[2]*Department of Physics, South University of Science and Technology of China, Shenzhen, Guangdong 518055, China*

[3]*Department of Chemistry, Princeton University, Princeton, New Jersey 08544, USA*

[4]*Center for Condensed Matter Sciences, National Taiwan University, Taipei 10617, Taiwan*

[5]*Department of Physics, National Tsing Hua University, Hsinchu 30013, Taiwan*

[6]*MAX-lab, Lund University, S-22100 Lund, Sweden*

[7]*Hiroshima Synchrotron Radiation Center, Hiroshima University, 2-313 Kagamiyama, Higashi-Hiroshima 739-0046, Japan*

[8]*Institute of Physics, Academia Sinica, Taipei 11529, Taiwan*

[9]*Department of Physics, National Sun Yat-Sen University, Kaohsiung 804, Taiwan*

[10]*Department of Physics, Northeastern University, Boston, Massachusetts 02115, USA*

[11]*Graphene Research Centre and Department of Physics, National University of Singapore 11754, Singapore*

(Received 15 December 2014; revised manuscript received 24 February 2015; published 10 August 2015)

A three-dimensional (3D) Dirac semimetal is a novel state of quantum matter which has recently attracted much attention as an apparent 3D version of graphene. In this paper, we report results on the electronic structure of the 3D Dirac semimetal Na_3Bi at a surface that reveals its nontrivial ground state. Our studies reveal that the two 3D Dirac cones go through a topological change in the constant energy contour as a function of the binding energy, featuring a Lifshitz point, which is missing in a strict 3D analog of graphene. Our results identify an example of a band saddle-point singularity in 3D Dirac materials. This is in contrast to its two-dimensional analogs such as graphene and the Dirac surface states of a topological insulator. The observation of multiple Dirac nodes in Na_3Bi connecting via a Lifshitz point along its crystalline rotational axis away from the Kramers point serves as a decisive signature for the symmetry-protected nature of the Dirac semimetal's topological *bulk* ground state.

DOI: 10.1103/PhysRevB.92.075115 PACS number(s): 73.20.At, 03.65.Vf, 03.65.Pm, 79.60.Bm

I. INTRODUCTION

Three-dimensional (3D) Dirac semimetals are materials whose bulk band structure features 3D Dirac fermion quasiparticles [1–14]. It was theoretically predicted that a 3D Dirac semimetal state can be realized at the critical point of the topological phase transition between a band insulator and a 3D topological insulator in a space inversion symmetric bulk crystal [2]. The Dirac semimetal state realized in this way features a single 3D Dirac cone at the Kramers point where the bulk band inversion occurs [2]. This type of 3D Dirac semimetal has been realized and observed in multiple material systems such as $BiTl(S_{0.5}Se_{0.5})_2$ and $(Bi_{0.94}In_{0.06})_2Se_3$ [13,15]. However, this approach requires fine-tuning the chemical doping/alloying composition, which is difficult to control and also introduces chemical disorders limiting the mobility of the system. In 2012 and 2013, numerical band calculations predicted 3D Dirac semimetal states in two stoichiometric materials, Na_3Bi and Cd_3As_2 [5,6]. Unlike the fine-tuned case, the Dirac semimetal states in Na_3Bi and Cd_3As_2 show a pair of bulk Dirac nodes that are located along the rotation axis away from the Kramers point in calculation [5,6]. This new type of Dirac semimetal with multiple bulk Dirac nodes arises from the protection by additional crystalline rotational symmetries [5–7]. They are believed to be stable within a range of material parameter space and robust to finite disorder or chemical doping. As a result, symmetry-protected Dirac semimetal states have soon attracted much interest [5–7]. Following these two band structure predictions, several photoemission experiments studied the (001) surface electronic structure of Na_3Bi and Cd_3As_2 [16–18]. Although 3D Dirac cones have been observed in both materials [16–18], it was found difficult to resolve the existence of two bulk Dirac cones and their overlap/interplay in momentum space when studying the (001) surface. Therefore, the critically important unique features of the electronic structure of symmetry-protected Dirac semimetals have not been unambiguously probed in experiments. Revealing the true electronic ground state is fundamental for future works on any new quantum materials, either theoretically or experimentally. This is even more important for a symmetry-protected Dirac semimetal such as Na_3Bi because it is the phenomenon of multiple bulk Dirac nodes away from the Kramers point along the rotation axis that distinguishes this new type of symmetry-protected Dirac semimetal state from the former (fine-tuned) type that is achieved by fine-tuning [7].

In this paper, we solve this problem by studying the electronic structure of Na_3Bi at a different surface—the (100) surface by angle-resolved photoemission spectroscopy (ARPES). The (001) and the (100) surfaces correspond to the (0001) and the $(10\bar{1}0)$ surfaces in the hexagonal four-index scheme. Our studies reveal unambiguously that the electronic ground state Dirac semimetal material Na_3Bi consists of two 3D Dirac cones and that these two Dirac cones go through a Lifshitz transition, a topological change in the constant energy contour [19], which is missing in a strict 3D analog of graphene. Our results identify an example of Van Hove singularity in a 3D Dirac system, and therefore pave the way for studying unusual phenomena related to Van Hove

singularities in these novel materials. These observations are made possible because we were able to access the (100) surface. At the (001) surface (as the case in previous studies [16–18]), the experiments were limited by the out-of-plane momentum resolution of ARPES probes.

II. METHODS

High quality single crystals of Na_3Bi were grown by a method reported in Ref. [20]. Ultraviolet spin-integrated ARPES measurements were performed at the beamline I4 at the MAX-lab in Lund in Sweden and the ESPRESSO endstation installed at the beamline-9B of the Hiroshima Synchrotron Radiation Center (HiSOR) in Hiroshima in Japan. The energy and momentum resolution was better than 30 meV and 1% of the Brillouin zone (BZ) for spin-integrated ARPES measurements at the beamline I4 at the MAX-lab and the ESPRESSO endstation at the beamline-9B of Hisor. Samples were cleaved *in situ* under a vacuum condition better than 1×10^{-10} Torr at all beamlines. Since bismuth trisodium is air sensitive, argon-filled gloveboxes with residual oxygen and water level less than 1 ppm were used in the entire preparation process. ARPES measurements were performed at liquid nitrogen temperatures in the I4 beamline at the MAX-lab, and at 10–20 K at the beamline 9B at HiSOR. Samples were found to be stable and without degradation for a typical measurement period of 24 h. The first-principles calculations were based on the generalized gradient approximation (GGA) [21] using the full-potential projected augmented wave method as implemented in the VASP package. Experimental lattice parameters were adopted from Ref. [20]. The electronic structure of bulk bismuth trisodium was calculated using a $9 \times 5 \times 5$ Monkhorst-Pack k mesh over the BZ with the inclusion of spin-orbit coupling.

III. RESULTS AND DISCUSSION

Na_3Bi crystallizes in the hexagonal $P6_3/mmc$ crystal structure with $a = 5.448$ Å and $c = 9.655$ Å [22] ($a^{-1}/c^{-1} \simeq 1.8$). It is a layered structure consisting of a honeycomb atomic plane where the Na and Bi atoms are situated on the A and B sites, respectively, sandwiched by layers of Na atoms which form a triangular lattice [see Figs. 1(a) and 1(b)]. In the ionic

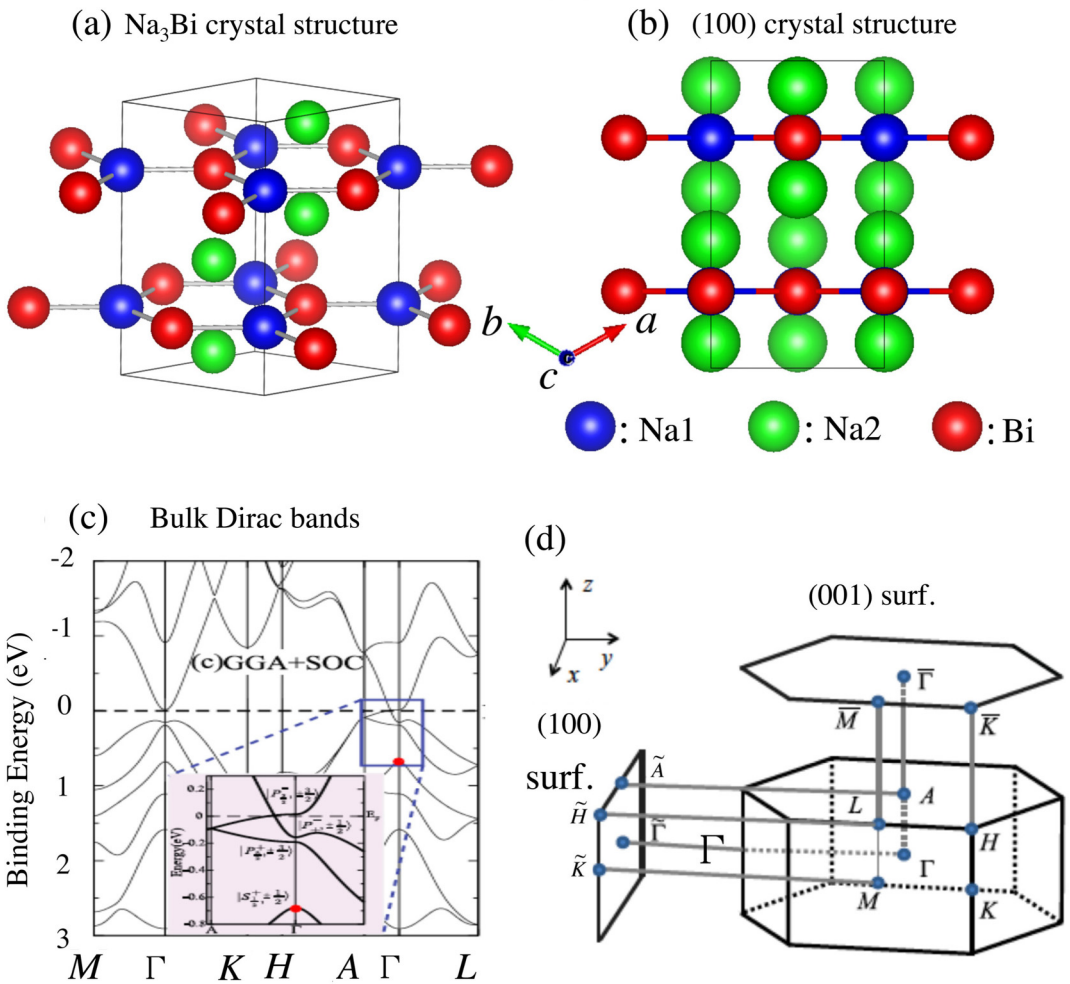

FIG. 1. (Color online) Crystal structure and multiple Dirac nodes in Na_3Bi. Characterization of Na_3Bi system. (a) Crystal structure of Na_3Bi. The two Na sites and Bi atoms are marked with different colors. (b) Projected crystal structure at the (100) surface. (d) First-principles bulk band structure calculation. (d) Structure of bulk and surface Brillouin zone at (001) and (100) surfaces. Bulk Dirac nodes are marked by green crosses. Panels (c) and (d) are adapted from Ref. [5].

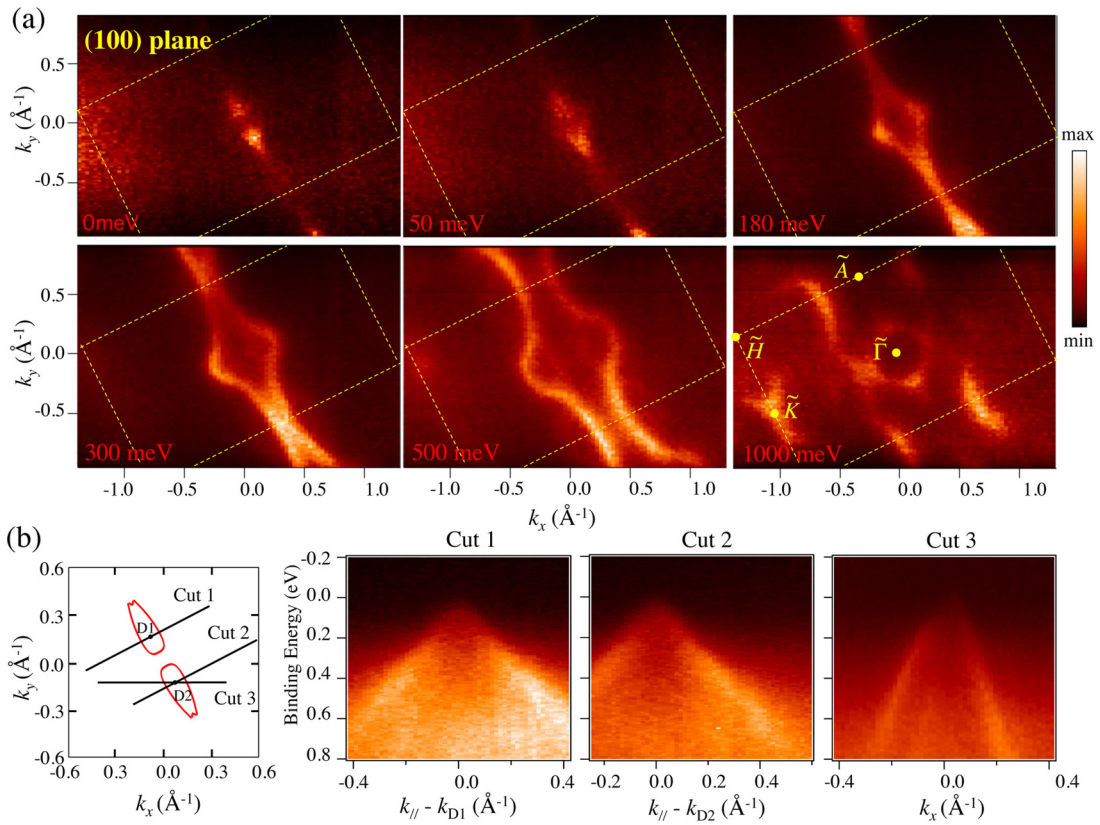

FIG. 2. (Color online) ARPES observation of multiple bulk Dirac cones. (a) ARPES constant energy maps obtained at the (100) surface using incident photon energy of 58 eV. Yellow dashed boxes indicate the surface Brillouin zone; notations of high symmetry points are shown at the $E_B = 1000$ meV panel; binding energies are marked in red on the lower left corner of each panel. (b) Selected ARPES k-E cuts, directions, and rough k ranges of the cuts are indicated by black solid lines in the left panel.

limit, the bulk conduction and valence bands are expected to be the Na 3s and the Bi 6$p_{x,y,z}$, respectively. However, first-principles calculation with spin-orbit interaction [5] shows that the conduction and valence bands are inverted at the bulk BZ center Γ point. Since the [001] axis (Γ-A direction in momentum space) is a C_3 rotational axis, all electronic bands along the Γ-A direction consist of states which are eigenstates of the C_3 rotational operator. Interestingly, in Na_3Bi, the lowest conduction and valence bands that go through the band inversion at the Γ point are found to have different C_3 eigenvalues [5,7]. This fact suggests that an energy gap cannot open between these two bands along the Γ-A direction even after including spin-orbit interaction. Consequently, two bulk Dirac band crossings along the A-Γ-A direction on the opposite sides of the Γ point are shown in first-principles calculations [Fig. 1(c)]. Therefore, the two bulk Dirac points are expected to be located along the [001] axis [5,6], which is perpendicular to the (001) surface [16–18]. Since the out-of-plane momentum resolution of ARPES is much limited, it is difficult to resolve the existence of two bulk Dirac cones and their overlap/interplay at the (001) surface. By contrast, they project onto different points in the (100) surface BZ [Fig. 1(d)].

Figure 2 shows our measured energy-momentum dispersion of the two bulk Dirac cones at the (100) surface. The ARPES constant energy maps are shown in Fig. 2(a). The surface BZ is found to be in a rectangular shape, which is consistent with the (100) surface termination. The length ratio between the long and short edges of the surface BZ (yellow boxes) is measured to be about $1.8 \simeq a^{-1}/c^{-1}$, also consistent with a (100) cleaving surface. Remarkably, at the Fermi level, our data clearly show that the Fermi surface consists of two unconnected band contours, which represent the two bulk Dirac cones. And the two bulk Dirac cones are observed to be equally spaced on the opposite sides of the Γ point along the A-Γ-A direction. A slight increase of binding energy up to 50 meV results in enlargement of the two Fermi pockets. At higher binding energies these two cones merge. The band contour further expands to form a neck region around the $\tilde{A}$ points (top of the 3D BZ). The chemical potential seems to be slightly below the energy of the two Dirac points, since the observed two separated pockets still have some finite area. Figure 2(b) presents several typical ARPES k-E maps along various cutting directions [black solid lines in the left panel of Fig. 2(b)]. A clear linear dispersion is seen for the bulk Dirac cones in all of these maps, establishing the existence of massless bulk quasiparticles. In Fig. 3 we study the band dispersion along the out-of-plane direction that is perpendicular to the (100) cleavage surface, by varying the incident photon energies of the synchrotron radiation. We expect the constant energy (k_y-k_z) maps to demonstrate an enlarging, circularlike band contour. From Fig. 3(a) one realizes that this is indeed the case. Moreover, the E-k_z (E-$k_{[100]}$) cut shown in Fig. 3(c) is also consistent with the expected linear dispersion. In Fig. 3(d) the same fact is emphasized again by showing the

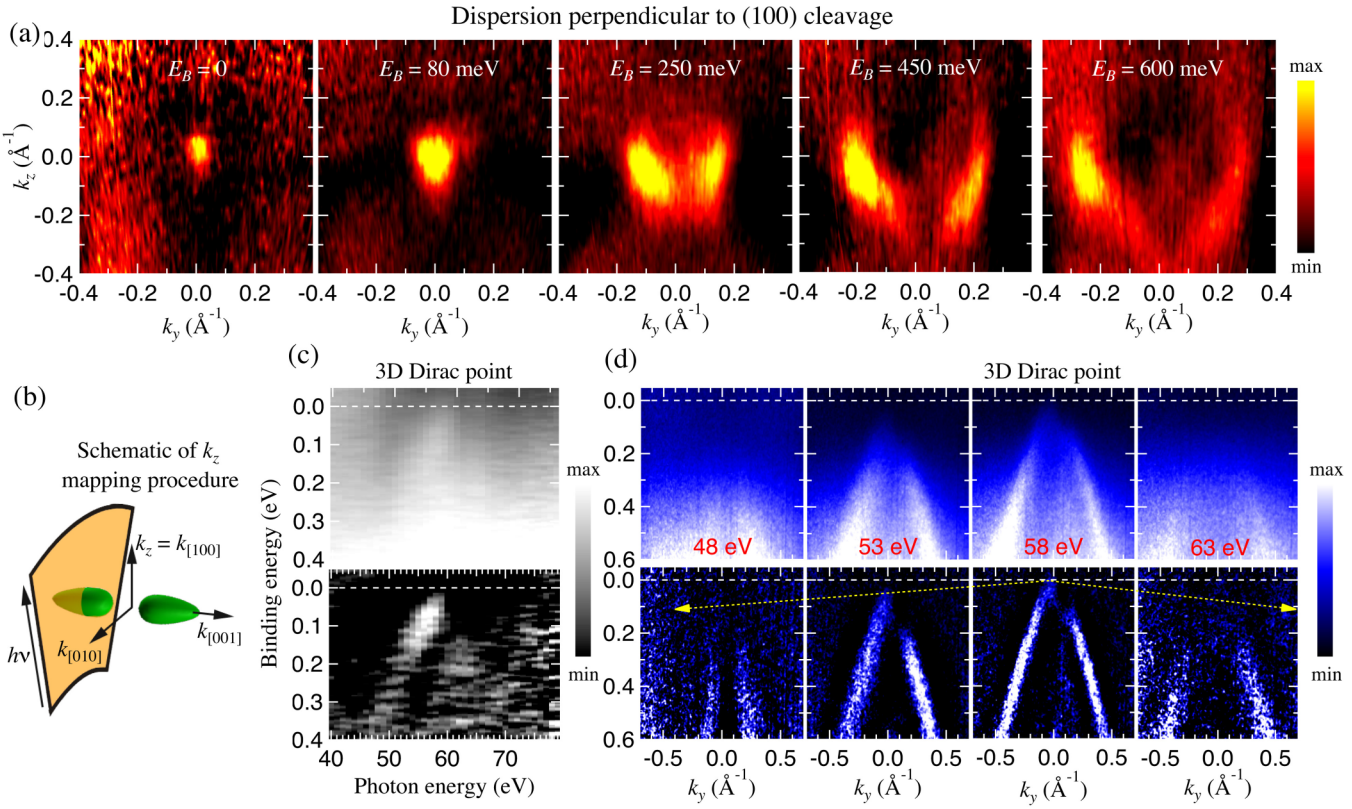

FIG. 3. (Color online) Out-of-plane dispersion of the bulk Dirac fermions. (a) ARPES constant energy maps along the k_y-k_z plane. Binding energies are marked on top of each panel. The k_z [100] axis is built by measuring ARPES k-E maps with photon energies ranging from 40 to 76 eV. (b) Schematic diagram of the k_z mapping procedure. Since the cleaving surface is (100), k_z corresponds to the [100] direction parallel to the crystallographic a axis. (c) Linear dispersion along the third dimension (k_z). Probing with different photon energies, the top of one of the bulk Dirac cones locate at different binding energies, constructing the linear k_z dispersion. (d) Linear k_z dispersion seen from in-plane k-E cuts. It is clear from the data that the bulk Dirac cone does not touch the Fermi level except for $h\nu = 58$ eV, consistent with the three-dimensional Dirac dispersion. For panels (c) and (d), the top row presents raw data and the bottom row shows second derivative results along the momentum distribution curves.

k_y-E maps for multiple photon energies. One realizes from Fig. 3(d) that the Dirac band touches the Fermi level only at $h\nu = 58$ eV.

Since the two bulk Dirac cones are located very close to one another in momentum space, they inevitably touch and hybridize with each other, giving rise to a topological change in the band contours, also known as a Lifshitz transition in the electronic structure. Figure 4 demonstrates our systematic ARPES investigation on the Lifshitz transition as well as the associated saddle-point band structure. Figure 4(a) presents a set of ARPES constant energy maps with higher momentum resolution than the one shown in Fig. 2. Besides the two bulk Dirac cones presented already in Fig. 2, we emphasize here the change of band structure where the two unconnected Dirac band contours merge. Experimentally, this Lifshitz transition happens at a binding energy of ~144 meV, at which the two holelike bands transform to a diamond-shaped loop. At higher binding energies, this loop enlarges while another concentric contour starts to appear at the zone center. This trend of band evolution is nicely reproduced in first-principles band calculations, as shown in Fig. 4(b) where a set of 3D ($k_{[100]}$,$k_{[010]}$,$k_{[001]}$) constant energy maps at selected binding energies are presented. The theoretical critical point of the Lifshitz transition is at $E_B = 134$ meV, only 10 meV away from the experimentally observed value. This slight energy difference between theory and experiment is entirely reasonable and it does not change our main conclusion. Note that our experimental energy resolution is >15 meV and first-principles (GGA) calculations may slightly underestimate the band gap. It can be seen in Fig. 4(a) that the two cones touch at two special momenta, $(k_x,k_y) = (\pm 0.1,0)$ Å^{-1}. To directly identify the saddle-point band structure as a result of the Lifshitz transition in experiments, we center our ARPES detector at one of the special momenta at $(k_x,k_y) = (+0.1,0)$ Å^{-1} and study two k-E maps, namely, cuts X and Y as defined in the third panel in Fig. 4(a). As shown in Fig. 4(d), the hybridized band reaches its local energy maximum at $(k_x,k_y) = (+0.1,0)$ Å^{-1} along k_x, while reaching a local energy minimum along k_y. This behavior defines a saddle-point singularity of band structure. At Fig. 4(e), an increase of local density of state (DOS) is observed by integrating the ARPES intensity around the saddle point, consistent with a local DOS maximum in a saddle-point type of Van Hove singularity in three dimensions. In Fig. 4(c) we compare and contrast the Lifshitz transition observed here with that observed in the surface states of a topological crystalline insulator (TCI) $Pb_{0.7}Sn_{0.3}Se$. In the n-typed sample of $Pb_{0.7}Sn_{0.3}Se$, the two *surface* Dirac cones hybridize at $E_B = 23$ and 96 meV. The difference between these two cases

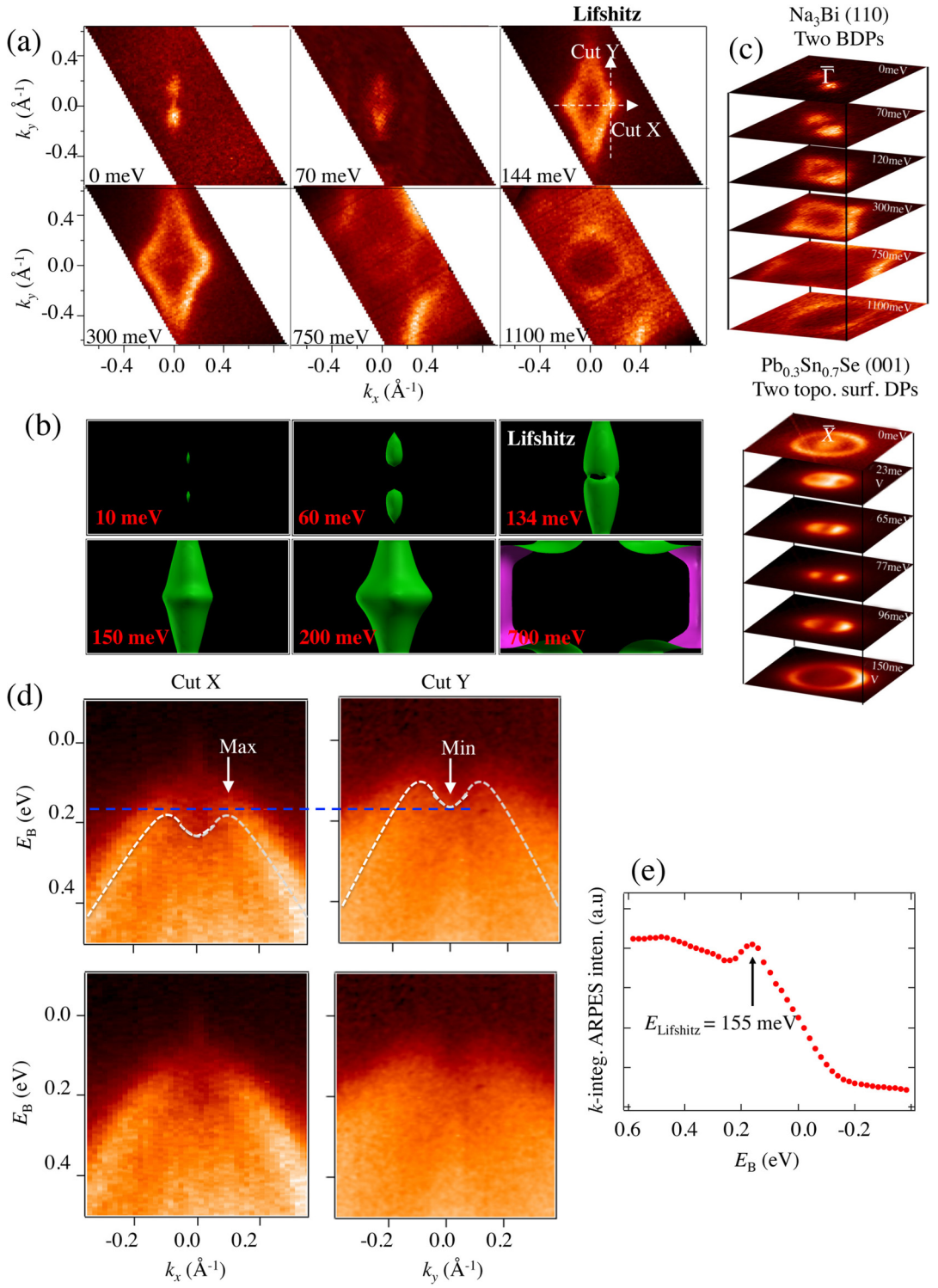

FIG. 4. (Color online) Lifshitz transition and saddle-point singularity in the bulk Dirac cones. (a) Lifshitz transition observed in ARPES constant energy maps. At $E_B \sim 144$ meV the two cones touch and hybridize to form a diamond-shaped single band contour, marking the Lifshitz transition. (b) Theoretical 3D constant energy maps at various binding energies, for comparison with panel (a). The inset in the 134 meV panel shows band projections onto the (100) surface at the Lifshitz energy. CEM: constant energy map. (c) Lifshitz transition of *bulk* Dirac fermions in Na_3Bi (top panel), compared with the Lifshitz transition of *surface* Dirac gas in a topological crystalline insulator $Pb_{0.7}Sn_{0.3}Se$ (bottom panel). (d) ARPES k-E maps along cut X and cut Y defined in panel (a) with and without the dashed lines. The dashed lines are guides to the eyes, which are drawn to only show the trend of the band dispersion at a qualitative level. (e) Saddle-point singularity observed from an anomalous increase of local density of states. The peak of integrated ARPES intensity marks the Lifshitz transition at $E_B \sim 155$ meV. The energy distribution curve is obtained by integrating the ARPES intensity at a (± 0.1 Å^{-1}, ± 0.1 Å^{-1}) window in the vicinity of the saddle point, which is the point where cut X and cut Y cross each other in panel (a).

is that for Na_3Bi, bulk Dirac quasiparticles, instead of the surface Dirac electron gas in the case of the TCI, merge and hybridize.

We note the following observations in our experiments: (i) we observe a pair of bulk Dirac nodes; (ii) they are located along the $C_3\, k_{[001]}$ axis away from the Γ point; (iii) the distance between the two in momentum space is only 0.2 $Å^{-1}$; and (iv) the Lifshitz transition and saddle-point singularity between the two are resolved. These observations are made possible because we studied the (100) surface. At the (001) surface [16–18], it is difficult due to the fact that the out-of-plane momentum resolution of ARPES is quite limited. We discuss the connection and distinction between the saddle-point type of Van Hove singularities in two-dimensional (2D) and 3D band structures. Saddle-point singularities in a 2D Dirac electron gas have been extensively studied in twisted bilayer graphene [23,24] and the surfaces of topological crystalline insulators [25]. In 2D, the DOS at the energy of the singularity diverges in a logarithmic fashion leading to electronic instability and correlated physics. In contrast, in 3D, the DOS itself reaches a finite maximum, but the derivative of the DOS does diverge. However, unconventional correlation physics can still arise if the bulk band structure is in a good quasi-2D approximation, such as the case in high-T_c copper superconductors [26]. Despite this difference, our results identify an example of band structure singularity in 3D Dirac materials. Moreover, we note that strictly speaking, Lifshitz transitions are topological changes of the Fermi surface upon changing some external parameter (doping, pressure, temperature, etc.). Thus to achieve such a Lifshitz transition and to access the singularity at the Fermi level, one needs to dope Na_3Bi to tune the chemical potential. A recent paper showed that controlling the chemical potential is indeed possible by finely adjusting the growth conditions of Na_3Bi [27,28]. Furthermore, we note that a very recent theory work has classified all possible 3D Dirac semimetal states [7]: theoretically, there are three classes of Dirac semimetals [7], namely, the (trivial) Dirac semimetal realized at the critical point of a topological phase transition, the (topological) Dirac semimetal state with a pair of Dirac nodes protected by the rotational symmetry, and the single-Dirac-cone Dirac semimetal state at the Kramers point protected by rotational symmetry. Our unambiguous observation of a pair of bulk Dirac nodes along the crystalline rotational axis away from the Kramers Γ point serves as a signature for the symmetry-protected nature of the Dirac semimetal state, and revealed that the ground state of Na_3Bi is a *nontrivial* 3D generalization of graphene.

Note added: During the review process of this paper, the first Weyl semimetal was experimentally discovered in TaAs [29,30]. This can be qualitatively understood as a topological Dirac semimetal such as Na_3Bi with its inversion symmetry broken, which gives rise to a new topological state with a new topological number [29,30].

ACKNOWLEDGMENTS

Work at Princeton University and Princeton-led synchrotron-based ARPES measurements were supported by the Gordon and Betty Moore Foundations EPiQS Initiative through Grant No. GBMF4547 (M.Z.H.) and by the U.S. National Science Foundation Grant No. NSF-DMR-1006492. First-principles band structure calculations at National University of Singapore were supported by the National Research Foundation, Prime Minister's Office, Singapore under its NRF fellowship (NRF Award No. NRF-NRFF2013-03). Single crystal growth at Princeton University was supported by the ARO MURI on Topological Insulators, Grant No. W911NF-12-1-0461. T.R.C. and H.T.J. were supported by the National Science Council, Taiwan. H.T.J. also thanks National Center for High-Performance Computing (NCHC), Computer and Information Network Center- National Taiwan University (CINC-NTU), and National Center for Theoretical Sciences (NCTS), Taiwan, for technical support. The work at Northeastern University was supported by the U.S. Department of Energy (DOE), Office of Science, Basic Energy Sciences Grant No. DE-FG02-07ER46352, and benefited from Northeastern University's Advanced Scientific Computation Center (ASCC) and the NERSC supercomputing center through DOE Grant No. DE-AC02-05CH11231. The work at MAX-lab was supported by the Swedish Research Council and Knut and Alice Wallenberg foundation. The work at Hisor was carried out through the external/international facility user program under the Proposal No. in HiSOR.14-A-23, and was supported by the KAKENHI (23244066) and the Grant-in-Aid for Scientific Research (A) of Japan Society for the Promotion of Science. We thank Chen Fang for discussions.

S.-Y. X. and C. L. contributed equally to this work.

[1] G. E. Volovik, *The Universe in a Helium Droplet* (Clarendon, Oxford, 2003).
[2] S. Murakami, New J. Phys. **9**, 356 (2007).
[3] H. Weyl, Z. Phys. **56**, 330 (1929).
[4] S. M.Young, S. Zaheer, J. C. Y. Teo, C. L. Kane, E. J. Mele, and A. M. Rappe, Phys. Rev. Lett. **108**, 140405 (2012).
[5] Z. Wang, Y. Sun, X.-Q. Chen, C. Franchini, G. Xu, H. Weng, Xi Dai, and Z. Fang, Phys. Rev. B **85**, 195320 (2012).
[6] Z. Wang, H. Weng, Q. Wu, X. Dai, and Z. Fang, Phys. Rev. B **88**, 125427 (2013).
[7] B.-J. Yang and N. Nagaosa, Nat. Commun. **5**, 4898 (2014).
[8] A. Narayan, D. Di Sante, S. Picozzi, and S. Sanvito, Phys. Rev. Lett. **113**, 256403 (2014).
[9] M. Z. Hasan and C. L. Kane, Rev. Mod. Phys. **82**, 3045 (2010).
[10] X.-L. Qi and S.-C. Zhang, Rev. Mod. Phys. **83**, 1057 (2011).
[11] D. Hsieh, D. Qian, L. Wray, Y. Xia, Y. S. Hor, R. J. Cava, and M. Z. Hasan, Nature (London) **452**, 970 (2008).
[12] Y. Xia, D. Qian, D. Hsieh, L. Wray, A. Pal, H. Lin, A. Bansil, D. Grauer, Y. S. Hor, R. J. Cava, and M. Z. Hasan, Nat. Phys. **5**, 398 (2009).

[13] S.-Y. Xu, Y. Xia, L. A. Wray, S. Jia, F. Meier, J. H. Dil, J. Osterwalder, B. Slomski, A. Bansil, H. Lin, R. J. Cava, and M. Z. Hasan, Science **332**, 560 (2011).
[14] S.-Y. Xu, N. Alidoust, I. Belopolski, A. Richardella, C. Liu, M. Neupane, G. Bian, S.-H. Huang, R. Sankar, C. Fang, B. Dellabetta, W. Dai, Q. Li, M. J. Gilbert, F.-C. Chou, N. Samarth, and M. Z. Hasan, Nat. Phys. **10**, 943 (2014).
[15] M. Brahlek, N. Bansal, N. Koirala, S.-Y. Xu, M. Neupane, C. Liu, M. Z. Hasan, and S. Oh, Phys. Rev. Lett. **109**, 186403 (2012).
[16] Z. K. Liu, B. Zhou, Y. Zhang, Z. J. Wang, H. M. Weng, D. Prabhakaran, S.-K. Mo, Z. X. Shen, Z. Fang, X. Dai, Z. Hussain, and Y. L. Chen, Science **343**, 864 (2014).
[17] M. Neupane, S.-Y. Xu, R. Sankar, N. Alidoust, G. Bian, C. Liu, I. Belopolski, T.-R. Chang, H.-T. Jeng, H. Lin, A. Bansil, F.-C. Chou, and M. Z. Hasan, Nat. Commun. **5**, 4786 (2014).
[18] S. Borisenko, Q. Gibson, D. Evtushinsky, V. Zabolotnyy, B. Büchner, and R. J. Cava, Phys. Rev. Lett. **113**, 027603 (2014).
[19] I. M. Lifshitz, Sov. Phys. JETP **11**, 1130 (1960).
[20] G. Brauer and E. Zintl, Z. Phys. Chem., Abt. B **37**, 323 (1937).
[21] J. P. Perdew, K. Burke, and M. Ernzerhof, Phys. Rev. Lett. **77**, 3865 (1996).
[22] T. B. Massalski, *Binary Alloy Phase Diagrams* (ASM, Materials Park, 1990).
[23] R. C. Dean, L. Wang, P. Maher, C. Forsythe, F. Ghahari, Y. Gao, J. Katoch, M. Ishigami, P. Moon, M. Koshino, T. Taniguchi, K. Watanabe, K. L. Shepard, J. Hone, and P. Kim, Nature (London) **497**, 598 (2013).
[24] L. A. Ponomarenko, R. V. Gorbachev, G. L. Yu, D. C. Elias, R. Jalil, A. A. Patel, A. Mishchenko, A. S. Mayorov, C. R. Woods, J. R. Wallbank, M. Mucha-Kruczynski, B. A. Piot, M. Potemski, I. V. Grigorieva, K. S. Novoselov, F. Guinea, V. I. Falko, and A. K. Geim, Nature (London) **497**, 594 (2013).
[25] M. Neupane, S.-Y. Xu, R. Sankar, Q. Gibson, Y. J. Wang, N. Alidoust, G. Bian, C. Liu, I. Belopolski, Y. Ohtsubo, A. Taleb-Ibrahimi, S. Basak, W.-F. Tsai, H. Lin, R. J. Cava, A. Bansil, F. C. Chou, and M. Z. Hasan, arXiv:1403.1560.
[26] J. E. Hirsch and D. J. Scalapino, Phys. Rev. Lett. **56**, 2732 (1986).
[27] S. Kushwaha, J. W. Krizan, B. E. Feldman, A. Gyenis, M. T. Randeria, J. Xiong, S.-Y. Xu, N. Alidoust, I. Belopolski, T. Liang, M. Z. Hasan, N. P. Ong, A. Yazdani, and R. J. Cava, APL Mater. **3**, 041504 (2015).
[28] S.-Y. Xu, C. Liu, S. K. Kushwaha, R. Sankar, J. W. Krizan, I. Belopolski, M. Neupane, G. Bian, N. Alidoust, T.-R. Chang, H.-T. Jeng, C.-Y. Huang, W.-F. Tsai, H. Lin, P. P. Shibayev, F.-C. Chou, R. J. Cava, and M. Z. Hasan, Science **347**, 294 (2015).
[29] S.-M. Huang, S.-Y. Xu, I. Belopolski, C.-C. Lee, G. Chang, B. Wang, N. Alidoust, G. Bian, M. Neupane, C. Zhang, S. Jia, A. Bansil, H. Lin, and M. Z. Hasan, Nature Commun. **6**, 7373 (2015).
[30] S.-Y. Xu, I. Belopolski, N. Alidoust, M. Neupane, G. Bian, C. Zhang, R. Sankar, G. Chang, Z. Yuan, C.-C. Lee, S.-M. Huang, H. Zheng, J. Ma, D. S. Sanchez, B. Wang, A. Bansil, F.-C. Chou, P. P. Shibayev, H. Lin, S. Jia, and M. Z. Hasan, Science (2015).